*J. Fluid Mech.* (2015), *vol.* 782, *pp.* 479–490.  
doi:10.1017/jfm.2015.568

# A scaling law for the lift of hovering insects

**Jeongsu Lee**[1], **Haecheon Choi**[1] **and Ho-Young Kim**[1,†]

[1]Department of Mechanical and Aerospace Engineering, Seoul National University, Seoul 08826, Korea

(Received 30 March 2015; revised 10 August 2015; accepted 22 September 2015)

Insect hovering is one of the most fascinating acrobatic flight modes in nature, and its aerodynamics has been intensively studied, mainly through computational approaches. While the numerical analyses have revealed detailed vortical structures around flapping wings and resulting forces for specific hovering conditions, theoretical understanding of a simple unified mechanism enabling the insects to be airborne is still incomplete. Here, we construct a scaling law for the lift of hovering insects through relatively simple scaling arguments of the strength of the leading edge vortex and the momentum induced by the vortical structure. Comparison of our theory with the measurement data of 35 species of insects confirms that the scaling law captures the essential physics of lift generation of hovering insects. Our results offer a simple yet powerful guideline for biologists who seek the evolutionary direction of the shape and kinematics of insect wings, and for engineers who design flapping-based micro air vehicles.

**Key words:** biological fluid dynamics, swimming/flying, vortex dynamics

## 1. Introduction

Insects can move more freely in air than most other creatures on Earth. In particular, insect hovering is one of the most fascinating acrobatic flight modes which has defied an explanation in terms of conventional aerodynamics for decades. Since a quasi-steady analysis of conventional aerodynamics was considered inappropriate for explaining the hovering dynamics (Ellington 1984*a*,*b*), unsteady mechanisms have been actively sought which can rationalize the aerodynamic force production through flapping. Several pioneering studies have found important unconventional mechanisms of hovering insects, such as the leading edge vortex (Ellington *et al.* 1996), wake capture and rotational mechanisms (Dickinson, Lehmann & Sane 1999).

Wing flaps of hovering insects can be largely decomposed into a translational mode and a rapid rotational stroke-reversal mode, which contribute to lift in different ways. The unusually large lift produced during the translational mode has been explained by a highly stabilized leading edge vortex that is attached to a wing even above a critical angle of attack (Ellington *et al.* 1996). It is during wing translation that most of the vertical force used to balance the weight of hovering insects is generated (Fry, Sayaman & Dickinson 2005; Liu & Aono 2009; Kweon & Choi 2010). It has been suggested that the wing rotation during stroke reversal produces instantaneous force

† Email address for correspondence: hyk@snu.ac.uk

peaks via the Kramer effect and interactions with previously existing wake structures (Dickinson *et al.* 1999; Sane & Dickinson 2002).

Further elaborated understanding of the flow fields around hovering insect wings has been achieved by recent flow measurement experiments (Poelma 2006; Lentink & Dickinson 2009; Cheng *et al.* 2013) and numerical simulations (Bos *et al.* 2008; Liu & Aono 2009). The leading edge vortex was shown to be stably attached in revolving conditions for the most relevant range of Reynolds numbers for insect hovering, $O(10^2)$–$O(10^4)$. The spiral leading edge vortex ensures low-pressure regions on the flapping wing, which enhance the lift. Three-dimensional digital particle image velocimetry (DPIV) experiments on a dynamically scaled model wing give a detailed picture of the vortical structures around the wing, where separation occurs all around the wing edges (Poelma 2006; Cheng *et al.* 2013). The separated vorticites form organized vortical structures, inducing the downward momentum responsible for the vertical force generated by flapping. Numerical simulations of hovering insects were shown to be consistent with the flow measurements on the model wing (Liu & Aono 2009). It was suggested that the tip vortices contribute to the aerodynamic lift by creating the low-pressure region near the wing tip and constructing the downward momentum (Shyy *et al.* 2009), in contrast to conventional aerodynamics where the tip vortex has a detrimental influence on the lift.

In searching for a simple model for the lift of hovering insects, the quasi-steady model was revised based on dynamically scaled model wing experiments (Dickinson *et al.* 1999; Sane & Dickinson 2002; Fry *et al.* 2005). In this model, the lift $L$ is written as $L = 0.5\rho U_R^2 S C_L(\alpha)$, where $U_R$ is the velocity of the radius of gyration, $S$ is the wing area, $C_L$ is the lift coefficient and $\alpha$ is the angle of attack. The lift coefficients are obtained using the force measurement data under steady wing velocity and angle of attack in experiments on revolving wings (Dickinson *et al.* 1999). The temporal evolution of the lift of hovering insects was reconstructed by the revised quasi-steady model.

However, we suggest that it should be further justified whether the force coefficient is the most suitable dimensionless parameter for flapping locomotion including insect hovering for the following reasons. In steady translation of the wing, the lift is a function of the fluid density $\rho$, viscosity $\mu$, wing velocity $U$, wing chord $c$, wing span $R$ and angle of attack $\alpha$. Then, dimensional analysis gives the following functional dependence of the dimensionless lift:

$$\frac{L}{\rho U^2 c^2} = \mathrm{fn}\left(\frac{\rho U c}{\mu}, \frac{R}{c}, \alpha\right), \tag{1.1}$$

where $L$ is the lift. For the lift coefficient defined as $C_L = L/(0.5\rho U^2 S)$ with $S = cR$, we obtain

$$C_L = \frac{c}{R}\mathrm{fn}\left(\frac{\rho U c}{\mu}, \frac{R}{c}, \alpha\right). \tag{1.2}$$

This tells us that steady translational wings of identical aspect ratio and angle of attack have the same lift coefficient regardless of change in velocity and area under the assumption that the ratio of inertia to viscous forces is large enough to neglect the effects of the Reynolds number, $Re = \rho U c/\mu$. Theoretical analysis also confirms that the lift coefficient is expressed as a function of the aspect ratio and angle of attack (Newman 1977). Hence, in steady translation of the wing, the lift coefficient is a suitable dimensionless parameter to interpret the dimensionless lift of various wings of different speed and area.

On the other hand, the lift of the wings in flapping conditions is a function of the flapping frequency $n$ and flapping amplitude $\Phi$ as well as $\rho$, $\mu$, $U$, $c$, $R$ and $\alpha$. Dimensional analysis yields

$$\frac{L}{\rho U^2 c^2} = \mathrm{fn}\left(\frac{\rho U c}{\mu}, \frac{R}{c}, \alpha, \frac{cn}{U}, \Phi\right). \tag{1.3}$$

Therefore, $C_L$ is written as

$$C_L = \frac{c}{R}\mathrm{fn}\left(\frac{\rho U c}{\mu}, \frac{R}{c}, \alpha, \frac{cn}{U}, \Phi\right). \tag{1.4}$$

In contrast to steady translational wings, wings at the same angle of attack and aspect ratio can have different lift coefficients under the influence of the reduced frequency ($cn/U$), which is a measure of the relative unsteadiness of the wing motion. In particular, for the wing flaps in hovering conditions, the reduced frequency can be written as $cn/U \sim cn/(R\Phi f) \sim c/(R\Phi)$ by assuming $U \sim R\Phi n$. The reduced frequency is then expressed as the ratio of the wing chord $c$ and the distance travelled $R\Phi$, which corresponds to the inverse of the Keulegan–Carpenter number (Keulegan & Carpenter 1958). Although the reduced frequency plays a significant role in oscillatory flows (Keulegan & Carpenter 1958; Dütsch *et al.* 1998; Jones 2003; Bidkar *et al.* 2009), its influence is not considered in the conventional model.

Actually, considerable inconsistency is found between the proposed lift coefficients even at the same angle of attack and aspect ratio depending on the experimental conditions (Willmott & Ellington 1997*b*; Sane 2003; Lentink & Dickinson 2009). If $C_L$ is a function of $\alpha$ only, as treated in a revised quasi-steady model, the data should be gathered onto a single curve in a polar plot, which turns out not to be the case. This hints at an incomplete role of the lift coefficient in describing forces in flapping condition. Moreover, a recent publication exists which points out the problem of the conventional fluid-dynamic model in flapping locomotion. Dewey *et al.* (2013) showed that the thrust, $T$, of flapping propulsion cannot be adequately explained when using the conventional thrust coefficient $C_T = T/(0.5\rho U^2 S)$. The experimental data for flapping panels did not collapse onto a single curve when plotted using $C_T$ (figure 4*b* therein). Instead, using a novel dimensionless variable, $\widetilde{T} = T/(\rho R^2 c^2 n^2)$, the data were gathered onto a single trend curve (figure 8*a* therein). We will show that the novel dimensionless variable proposed by Dewey *et al.* (2013) is consistent with our scaling law for the lift in the following.

In this regard, we seek a simple theory to estimate the forces that enable insects to be airborne without resorting to empirical lift coefficients. We construct a scaling law for the lift of hovering insects as a function of their morphological and kinematic parameters. The simple physical understanding obtained through this work can help one to elucidate the evolutionary pressure of shape and kinematics of insect wings, and to establish design rules for flapping-based micro air vehicles.

We first revisit conventional aerodynamics to check its relevance. In the conventional steady potential-flow theory, the lift of a wing is obtained by the following two steps. First, the flow field around the wing is determined by the continuity equation and the boundary conditions composed of a kinematic boundary condition on the wing surface, a smooth flow-off requirement at the trailing edge and the far-field velocity. These kinematic relations give the velocity field and instantaneous circulation around the wing. Second, the Kutta–Joukowski theorem gives the lift of the wing as the

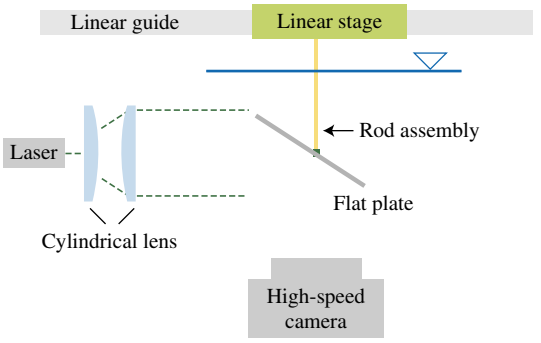


FIGURE 1. (Colour online) Experimental apparatus to visualize the flow field.

product of the fluid density, the free-stream velocity and the circulation bound to the wing (Newman 1977). We suppose that the first kinematic step still holds for hovering insect wings because the separating flow is confined around the leading edge vortex and a smooth flow-off condition is recovered at the trailing edge (Birch & Dickinson 2003; Sane 2003). However, the second dynamic step is far from valid for hovering insect wings, which flap in a cyclic manner only after several chord lengths of travel. The separated vorticity of the leading and trailing edges remains in the vicinity of the wing during most of the stroke cycle (Poelma 2006; Liu & Aono 2009; Jardin *et al.* 2012). Instead of the Kutta–Joukowski theorem, we need to consider the momentum of the flow field induced by the vortical structures around the wing directly so as to model the lift.

In the following, therefore, we first approximate the instantaneous circulation of the leading edge vortex of hovering wings, which is assumed to play a dominant role in lift production, using the steady theory. We next measure the strength of the leading edge vortex of a dynamically scaled robot wing to test whether the steady aerodynamic theory provides a reasonable approximation for the strength of the leading edge vortex. We then construct a novel model for the momentum induced by the vortical structure around the wing, which eventually determines the lift. Our theory is tested by comparing the scaling law with the weight data for various species of insects.

## 2. Experimental apparatus

A rectangular rigid acrylic flat plate of 1 mm thickness is attached to a rod, which is driven by a linear stage (Newport IMS-LM), as shown in figure 1. The span of the plate is varied as 4, 6 and 8 cm and its chord is varied as 1.5, 2, 2.5, 3.5 and 4 cm. The flat plate and rod assembly is immersed in a water tank measuring 125, 15 and 25 cm in length, width and depth respectively. The free surface is 10 cm above the top of the flat plate. While the plate is linearly translated along the length of the water tank, the velocity varies sinusoidally to complete a half-period as $U(t) = U_0 \sin(\pi t/T)$ for the time interval $0 < t < T$, with $U_0$ being the maximum velocity. The velocity fields and vorticity contours are obtained by two-dimensional DPIV. Polyamide particles of 50 μm diameter are used as seeding particles. The central plane perpendicular to the plate is illuminated to visualize seeding particles with an 8 W continuous laser of 532 nm wavelength through a slit. The images captured by a high-speed camera (Photron APX-RS), consisting of $1024 \times 1024$ pixels,

are analysed to generate a velocity field with a $64 \times 64$ interrogation size and a 75 % overlap. The derived velocity vectors are validated by a dynamic mean value operator. The vorticity field is obtained using commercial graphic software based on the derived velocity field.

## 3. Results and discussion

### 3.1. *Estimation of leading edge vortex strength*

The shear flow separated at the leading edge of a hovering insect wing spirals into the leading edge vortex. Thus, the strength of the leading edge vortex is related to that of the shear flow generated on the wing, which is modelled as vortex sheets in the classical steady aerofoil theory. We scale the strength of the leading edge vortex via the circulation around a three-dimensional wing (Newman 1977), $\Gamma$, as

$$\Gamma \sim \frac{U\bar{c}\Lambda \sin\alpha}{\Lambda + 2}, \tag{3.1}$$

where $\sim$ signifies 'is scaled as', $U$ is the free-stream velocity, $\alpha$ is the angle of attack and $\bar{c}$ is the mean chord. Here, $\Lambda = R/\bar{c}$ is the aspect ratio, with $R$ being the wing span. To test whether the present model provides a reasonable approximation for the strength of the leading edge vortex on wings operated in hovering conditions, we measured the vorticity of flows around a flat plate translating linearly at high angles of attack within a water tank. The ranges of all independent parameters, such as wing velocity, stroke distance, angle of attack, wing span and chord, were selected to dynamically scale the characteristic values of the wings of hovering insects (see the supplementary data available at http://dx.doi.org/10.1017/jfm.2015.568). The Reynolds number, $Re = \rho U\bar{c}/\mu$, ranged from 200 to 3500, the dimensionless stroke amplitude ($A$, the ratio of stroke distance to mean chord) from 1.6 to 3.4, $\alpha$ from 25° to 70° and $\Lambda$ from 1.5 to 2.7.

Figure 2(*a*) displays the representative velocity field and the resulting vorticity contours. The leading edge vortex was identified using the criteria proposed by Jeong & Husssain (1995), as shown in figure 2(*b*). Figure 2(*c*) plots the measured instantaneous circulation in the leading edge vortex at $t = T/2$ during translation according to the scaling law (3.1) for 19 cases. All of the data collapse onto a straight line with a slope 3.06, which is very close to the value expected from conventional aerodynamics, $\pi$ (Newman 1977).

### 3.2. *A model for lift*

Now we move on to the lift of hovering insects by considering the momentum induced by the vortical structure generated by the wing stroke. Because the vortical structure around the wing is characterized as the vortex loop over the wing (Poelma 2006; Liu & Aono 2009; Jardin *et al.* 2012), we approximate the momentum induced by the vortical structure, $\Delta I$, as $\Delta I \sim \rho\Gamma S \sim \rho\Gamma R\bar{c}$ (Dickinson 1996; Wu *et al.* 2006; Lee *et al.* 2013). The reaction force exerted on the wing due to the time derivate of vortical impulse is scaled as $F \sim \Delta I/T \sim \rho\Gamma R\bar{c}/T$, which is perpendicular to the wing surface. Here, $T$ is the flapping period.

For the flapping translation of hovering insects, the linear velocity of the wing is scaled as $U \sim \Phi Rn$, with $\Phi$ and $n$ being the stroke amplitude and flapping frequency respectively. Thus, the circulation around the leading edge vortex can be scaled as $\Gamma \sim \Phi Rn\bar{c}\Lambda \sin\alpha/(\Lambda + 2)$ via the scaling relation (3.1). By combining these relations,

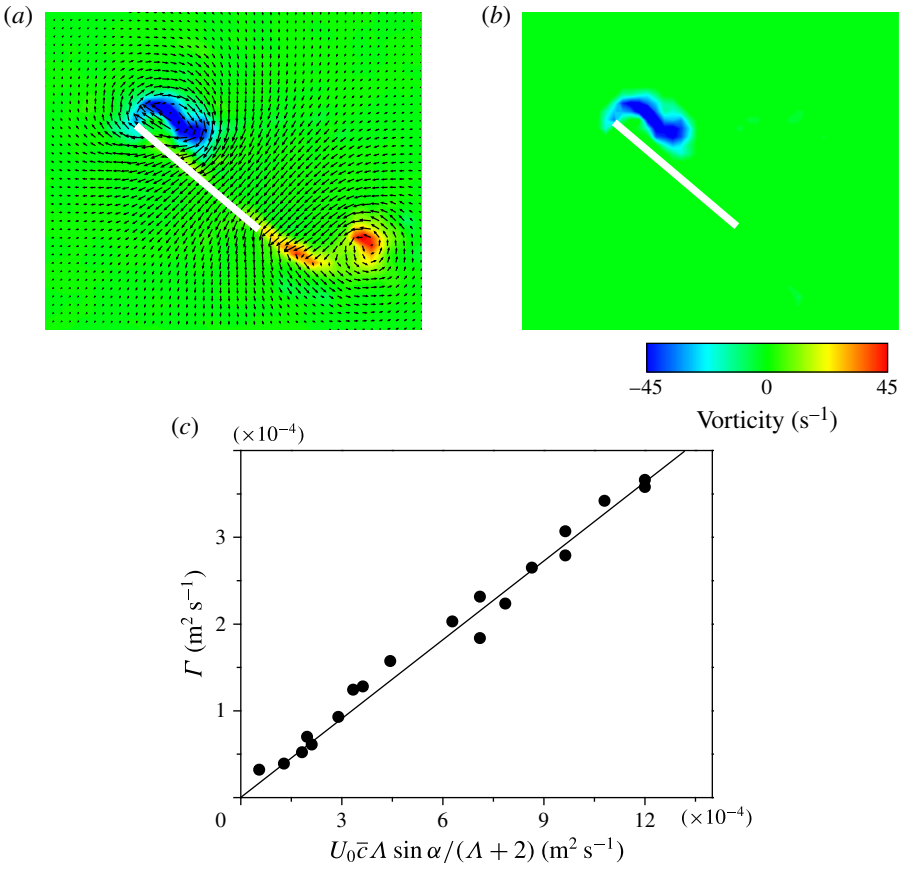


FIGURE 2. (Colour online) (*a*) Velocity field and vorticity contour around a translating wing with $Re = 2500$, $\alpha = 45$, $A = 1.7$ at $t = T/2$. (*b*) Isolated leading edge vortex around an identical wing. (*c*) Instantaneous circulation, $\Gamma$, of the leading edge vortex at $t = T/2$ versus the scaling parameter $U_0\bar{c}\Lambda \sin\alpha/(\Lambda+2)$.

we obtain the scaling approximations of lift and drag with respect to the stroke plane as $L \sim \rho\Phi R^2\bar{c}^2n^2\Lambda \sin\alpha\cos\alpha/(\Lambda+2)$ and $D \sim \rho\Phi R^2\bar{c}^2n^2\Lambda \sin^2\alpha/(\Lambda+2)$ respectively. The vertical component of the aerodynamic force produced balances the insect weight, $W$. The contribution of drag to the vertical component of the period-averaged aerodynamic force is very small compared with that of lift because the drags during up- and downstrokes cancel each other out except for dragonfly-like wing motions having severe asymmetry of up- and downstrokes (Wang 2004; Park & Choi 2012). By balancing the vertical component of the lift with the insect weight, we obtain

$$W \sim 0.5\rho\Phi R^2\bar{c}^2n^2\frac{\Lambda \sin 2\alpha}{\Lambda+2}\cos\beta, \tag{3.2}$$

where $\beta$ is the stroke plane angle, that is, the angle between the horizontal and stroke planes. We note that our scaling law for the lift is consistent with the novel dimensionless thrust proposed by Dewey *et al.* (2013), $L \sim \rho R^2c^2n^2\eta$, where $\eta$ is a function of geometrical parameters, as mentioned in § 1.

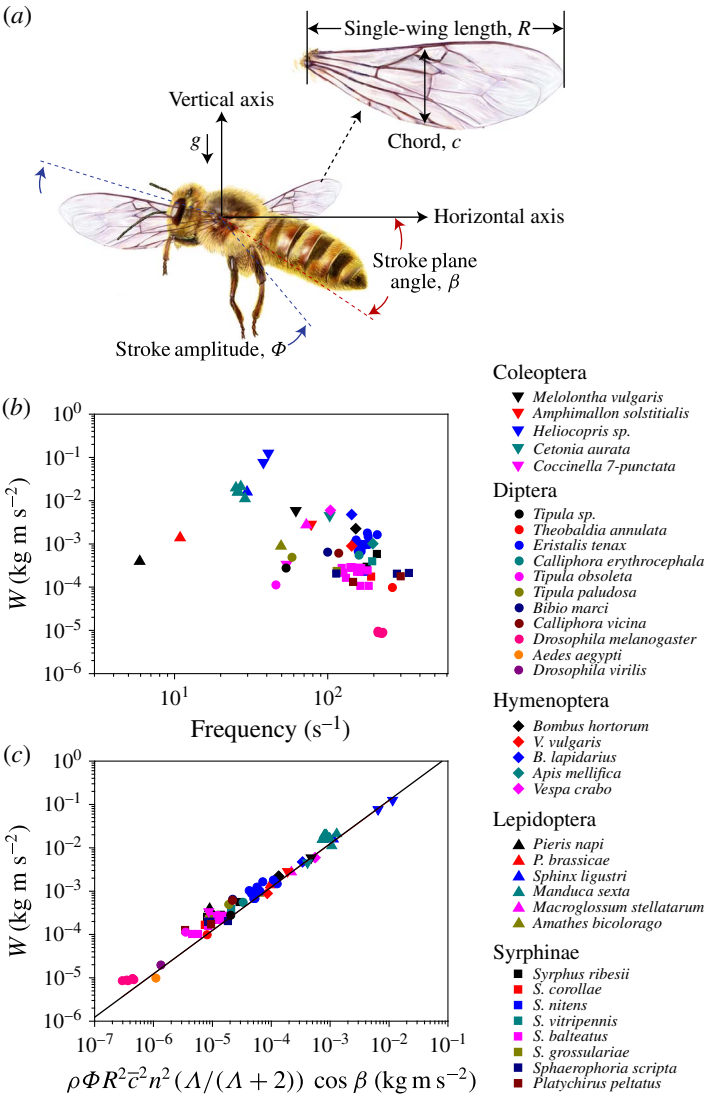


FIGURE 3. (*a*) Illustration to define morphological and kinematical parameters of hovering insects. (*b*,*c*) Weight of the insect versus (*b*) frequency and (*c*) the scaling parameter $\rho\Phi R^2\bar{c}^2n^2(\Lambda/(\Lambda+2))\cos\beta$. We compare our theory with experimental observations (83 data points) for 35 species of hovering insects (Weis-Fogh 1973; Ellington 1984*c*,*d*; Ennos 1989; Willmott & Ellington 1997*a*,*b*; Fry *et al.* 2005; Liu & Sun 2008; Walker *et al.* 2010; Mou, Liu & Sun 2011). In (*c*), the straight line corresponds to $y = 11.4x$.

We first compare our theory for lift with the data (see the supplementary data) for 35 species of hovering insects from previously published papers that report the wing dimensions, flapping frequency and body weight (Weis-Fogh 1973; Ellington 1984*c*,*d*; Ennos 1989; Willmott & Ellington 1997*a*,*b*; Fry *et al.* 2005; Liu & Sun 2008; Walker *et al.* 2010; Mou *et al.* 2011). While the raw data scatter considerably when plotted against one of the most influential factors in the force production, the flapping frequency, figure 3(*b*), the data plotted according to the scaling law collapse

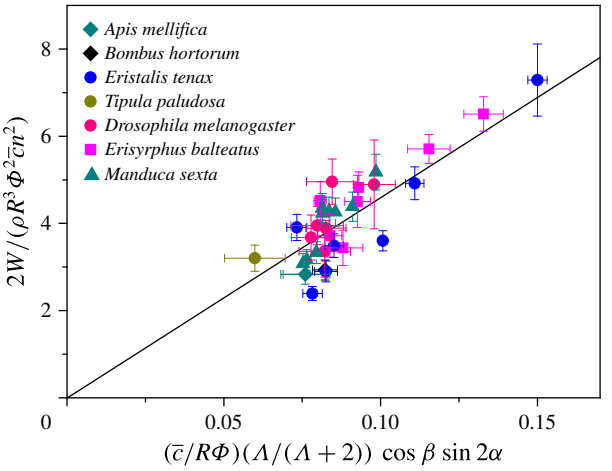


FIGURE 4. Experimental validation of the normalized scaling law, (3.3). We compare our theory with experimental observations (32 data points) for six species of hovering insects (Ellington 1984*c*,*d*; Willmott & Ellington 1997*a*,*b*; Fry *et al.* 2005; Liu & Sun 2008; Walker *et al.* 2010; Mou *et al.* 2011).

onto a master curve, figure 3(*c*). Since most of the experimental observations do not report the angle of attack, we have simply modified the scaling law by ignoring $\sin 2\alpha$. Considering that the right-hand side of equation (3.2) varies by up to six orders of magnitude without $\sin 2\alpha$, the variation of $\sin 2\alpha$ for different insects is indeed insignificant. It varies from 0.6 to 0.9 with the angle of attack changing from 20° to 60°. We validate our theory further with the data for six species of insects for which the angle of attack during each half-stroke is known (Ellington 1984*c*,*d*; Willmott & Ellington 1997*a*,*b*; Fry *et al.* 2005; Liu & Sun 2008; Walker *et al.* 2010; Mou *et al.* 2011). The weight of the insect normalized by the dynamic pressure force, $0.5\rho U^2 R\bar{c}$, with the characteristic wing tip velocity $U \sim \Phi Rn$ and the wing area $R\bar{c}$, is scaled as

$$\frac{2W}{\rho R^3 \Phi^2 \bar{c} n^2} \sim \frac{\bar{c}}{R\Phi}\frac{\Lambda}{\Lambda+2}\cos\beta\sin 2\alpha. \tag{3.3}$$

We plot the experimental data according to the dimensionless scaling law (3.3) in figure 4. The scaling law agrees favourably with the experimental observations, with the slope of the best-fitting straight line being 46.2.

Our analysis is distinguished from the conventional steady potential-flow theory in that the lift is scaled as $L \sim \rho\Gamma\bar{c}R/T$ rather than $L \sim \rho\Gamma UR$, with $U \sim \Phi Rn$ (see appendix A). This is mainly due to the difference in the vorticity generation process. The steady lift production arises from the formation of trailing vortices at wing tips (freely convecting chordwise vorticity), with its generation rate proportional to the translational velocity $U$ while the spanwise vortex sheet is bound to the wing surface. As a result, the evolution of the vortical structure around the steady wing can be modelled by a single vortex loop with a monotonically increasing area (Newman 1977; Dickinson 1996; Wu *et al.* 2006). In contrast, on a hovering insect wing, the vorticity is generated all around the edges, including the spanwise vorticity at the leading edge (Poelma 2006; Liu & Aono 2009). We have shown that it is the generation of spanwise vorticity along the wing edges that plays a crucial role in

producing lift for hovering insects. We also compare our theory and conventional theory with the lift measurement data for reciprocally translating wings given by Lentink & Dickinson (2009) in appendix B.

## 4. Conclusions

Our theory has been shown to successfully capture the dominant physical mechanism underlying the lift generation in hovering flight, allowing us to obtain a simple scaling law for the lift with given morphological and kinematic parameters of the insects. However, detailed fluid-dynamic phenomena associated with hovering, such as time-dependent flow structures, the force history and the interaction with the wake, can be adequately accounted for by numerically computing the full Navier–Stokes equation.

We believe that our theory will not only help one to grasp the essential aerodynamics of hovering easily but also shed light on some biological observations that have eluded scientific explanation based on conventional theory for decades (Ellington 1984*a*; Dickinson *et al.* 1999). For instance, the wing load, $W/(R\bar{c})$, of the hoverfly *Syrphus balteatus* is $\sim$8.97 N m$^{-2}$, which is similar to that of the crane fly *Tipula paludosa* ($\sim$9.11 N m$^{-2}$) despite dramatic differences in their wing size and kinematics (see the supplementary data). The stroke angle of the hoverfly wing ranges only from 60° to 70°, which is almost half of the typical stroke angle of many hovering insects including the crane fly. The wing chords of the two insects are similar (2.98 mm for the hoverfly and 3.09 mm for the crane fly), but the wingspan of the hoverfly, approximately 9.9 mm, is almost half that of the crane fly. However, the flapping frequency of the hoverfly (124 Hz), which is almost twice as high as that of the crane fly (58 Hz), successfully compensates for such disadvantages. Our theory allows us to explain this observation because $W/(R\bar{c})$ is proportional to $n^2$, but scales linearly with $R$ and $\Phi$: $W/(R\bar{c}) \sim n^2 R\Phi$. In other words, hoverflies flap their wings just fast enough to surmount the drawbacks of small stroke angle and wingspan. The conventional theory cannot account for this morphological and kinematic dependence because it predicts $W/(R\bar{c}) \sim n^2 R^2 \Phi^2$. Our theory provides a clear fluid-dynamic explanation of how different evolutionary selections for wing kinematics and morphology among insect species can arrive at the same functionality: hovering with similar wing loads. We also expect that our scaling law will be a simple yet powerful guideline for designing flapping-based micro air vehicles.

### Acknowledgements

This work was supported by the National Research Foundation of Korea (Grant nos. 2011-0028032, 2014048162 and 2014023206) via SNU IAMD.

### Supplementary data

Supplementary data is available at http://dx.doi.org/10.1017/jfm.2015.568.

### Appendix A. Scaling law based on the conventional steady potential-flow theory

In the conventional steady potential-flow theory, the lift and circulation of the leading edge vortex can be written as $L \sim \rho \Gamma U R$ and $\Gamma \sim U\bar{c}\Lambda \sin\alpha/(\Lambda + 2)$ respectively (Newman 1977; Dickinson 1996). Since the flapping velocity $U \sim \Phi R n$, the vertical force that balances the weight is scaled as

$$W \sim \rho \Phi^2 R^3 \bar{c} n^2 \frac{\Lambda}{\Lambda + 2} \sin\alpha \cos\beta. \tag{A 1}$$

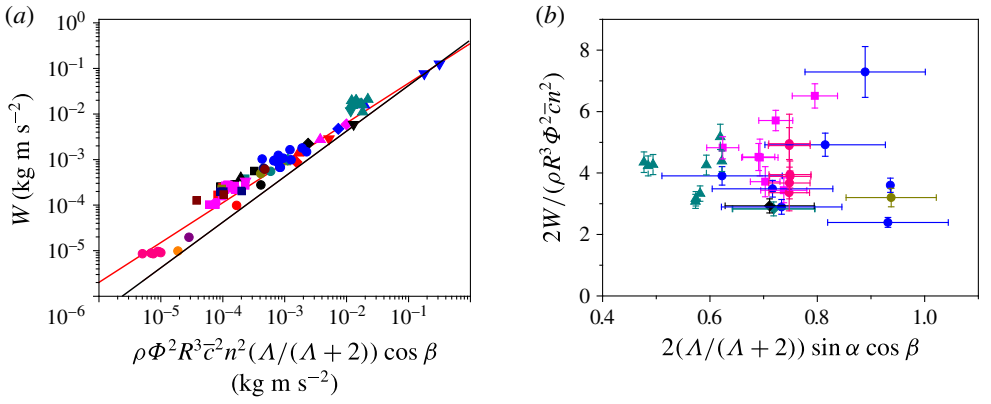


FIGURE 5. (Colour online) Experimentally measured weight of hovering insects plotted according to (*a*) scaling law (A 1) and (*b*) normalized scaling law (A 2) based on the conventional steady potential-flow theory. In (*a*), the black and red lines correspond to $y \sim x$ and $y \sim x^{0.87}$ respectively. The symbols are from figure 3.

The normalized form is given by

$$\frac{W}{\rho R^3 \Phi^2 \bar{c} n^2} \sim \frac{\Lambda}{\Lambda + 2} \sin\alpha \cos\beta. \tag{A 2}$$

We first plot the experimental data according to (A 1) in figure 5(*a*). The data appear to collapse onto a master curve with the conventional theory for an obvious reason that the pressure forces exerted on the wing would grow with the dynamic pressure and the surface area. However, investigation of the slopes of the lines reveals a significant difference between the plots using conventional theory (figure 5*a*) and our theory (figure 3*c*). For the conventional theory to hold, the data should collapse onto a line representing $y = ax$ in log–log plot, where $y$ and $x$ represent the values of the vertical and horizontal axes respectively. This is shown as a black line in the figure. Obviously, the biological data do not follow the line $y \sim x$. Rather, the least-square method finds the best-fitting line for the biological data to be $y \sim x^{0.87}$, the red line. This implies that the biological data are consistent with the following power law: $W \sim \left[\rho\Phi^2R^3\bar{c}^2n^2\cos\beta\Lambda/(\Lambda+2)\right]^{0.87}$, which has no theoretical background. We further plot the experimental data according to the normalized scaling law (A 2) in figure 5(*b*). The data are scattered rather than collapsing onto a single master curve as in figure 4.

## Appendix B. Comparison with previous experiments on flapping locomotion

We compare our theory and the conventional model with the lift measurement data for reciprocally translating wings given by Lentink & Dickinson (2009), as shown in figure 6. The lift increases linearly with our scaling law, figure 6(*a*), whereas the lift does not follow what the conventional theory predicts, figure 6(*b*). In more detail, the experimental data for $Re = 110$ (circles) and 1400 (triangles) were collected with the same velocity but by varying the density and viscosity of the fluid. For $Re =$ 14 000 (squares), the velocity of the wing and the physical properties of the fluid were altogether changed compared with the cases of $Re = 1400$ and 110. The data

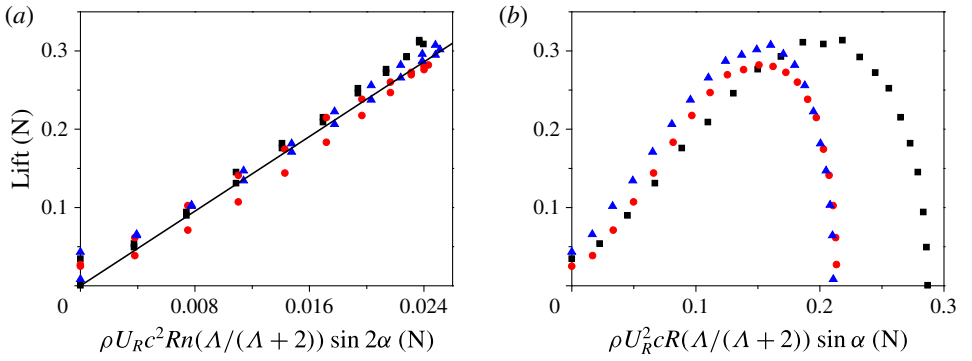


FIGURE 6. (Colour online) The experimentally measured lift of the reciprocally translating wing in Lentink & Dickinson (2009) plotted according to (*a*) our scaling law and (*b*) the conventional steady potential-flow theory. The circles, triangles and squares correspond to $Re = 110,\ 1400$ and $14\,000$.

plotted according to the conventional model show significant inconsistency when the wing velocity is changed, whereas all of the data collapse onto a single line when plotted according to our scaling law.

## REFERENCES

BIDKAR, R. A., KIMBER, M., RAMAN, A., BAJAJ, A. K. & GARIMELLA, S. V. 2009 Nonlinear aerodynamic damping of sharp-edged flexible beams oscillating at low Keulegan–Carpenter numbers. *J. Fluid Mech.* **634**, 269–289.

BIRCH, J. M. & DICKINSON, M. H. 2003 The influence of wing–wake interactions on the production of aerodynamic forces in flapping flight. *J. Expl Biol.* **206**, 2257–2272.

BOS, F. M., LENTINK, D., VAN OUDHEUSDEN, B. W. & BIJL, H. 2008 Influence of wing kinematics on aerodynamic performance in hovering insect flight. *J. Fluid Mech.* **594**, 341–368.

CHENG, B., SAND, S. P., BARBERA, G., TROOLIN, D. R., STRAND, T. & DENG, X. 2013 Three-dimensional flow visualization and vorticity dynamics in revolving wings. *Exp. Fluids* **54**, 1–12.

DEWEY, P. A., BOSCHITSCH, B. M., MOORED, K. W., STONE, H. A. & SMITS, A. J. 2013 Scaling laws for the thrust production of flexible pitching panels. *J. Fluid Mech.* **732**, 29–46.

DICKINSON, M. H. 1996 Unsteady mechanisms of force generation in aquatic and aerial locomotion. *Am. Zool.* **36**, 537–554.

DICKINSON, M. H., LEHMANN, F.-O. & SANE, S. P. 1999 Wing rotation and the aerodynamic basis of insect flight. *Science* **284**, 1954–1960.

DÜTSCH, H., DURST, F., BECKER, S. & LIENHART, H. 1998 Low-Reynolds-number flow around an oscillating circular cylinder at low Keulegan–Carpenter numbers. *J. Fluid Mech.* **360**, 249–271.

ELLINGTON, C. P. 1984*a* The aerodynamics of flapping animal flight. *Am. Zool.* **24**, 95–105.

ELLINGTON, C. P. 1984*b* The aerodynamics of hovering insect flight. Part I: the quasi-steady analysis. *Phil. Trans. R. Soc. Lond.* B **305**, 1–15.

ELLINGTON, C. P. 1984*c* The aerodynamics of hovering insect flight. Part II: morphological parameters. *Phil. Trans. R. Soc. Lond.* B **305**, 17–40.

ELLINGTON, C. P. 1984*d* The aerodynamics of hovering insect flight. Part III: kinematics. *Phil. Trans. R. Soc. Lond.* B **305**, 41–78.

ELLINGTON, C. P., VAN DEN BERG, C., WILLMOTT, A. P. & THOMAS, A. L. R. 1996 Leading-edge vortices in insect flight. *Nature* **384**, 626–630.

ENNOS, A. R. 1989 The kinematics and aerodynamics of the free flight of some Diptera. *J. Expl Biol.* **142**, 49–85.

FRY, S. N., SAYAMAN, R. & DICKINSON, M. H. 2005 The aerodynamics of hovering flight in Drosophila. *J. Expl Biol.* **208**, 2303–2318.

JARDIN, T., FARCY, A. & DAVID, L. 2012 Three-dimensional effects in hovering flapping flight. *J. Fluid Mech.* **702**, 102–125.

JEONG, J. & HUSSAIN, F. 1995 On the identification of a vortex. *J. Fluid Mech.* **285**, 69–94.

JONES, M. A. 2003 The separated flow of an inviscid fluid around a moving flat plate. *J. Fluid Mech.* **496**, 405–441.

KEULEGAN, G. H. & CARPENTER, L. H. 1958 Forces on cylinders and plates in an oscillating fluid. *J. Res. Natl Bur. Stand.* **60**, 423–440.

KWEON, J. & CHOI, H. 2010 Sectional lift coefficient of a flapping wing in hovering motion. *Phys. Fluids* **22**, 071703.

LEE, J., PARK, Y.-J., JEONG, U., CHO, K.-J. & KIM, H.-Y. 2013 Wake and thrust of an angularly reciprocating plate. *J. Fluid Mech.* **720**, 545–557.

LENTINK, D. & DICKINSON, M. H. 2009 Rotational accelerations stabilize leading edge vortices on revolving fly wings. *J. Expl Biol.* **212**, 2705–2719.

LIU, H. & AONO, H. 2009 Size effects on insect hovering aerodynamics: an integrated computational study. *Bioinspir. Biomim.* **4**, 015002.

LIU, Y. & SUN, M. 2008 Wing kinematics measurement and aerodynamics of hovering droneflies. *J. Expl Biol.* **211**, 2014–2025.

MOU, X. L., LIU, Y. P. & SUN, M. 2011 Wing motion measurement and aerodynamics of hovering true hoverflies. *J. Expl Biol.* **214**, 2832–2844.

NEWMAN, J. N. 1977 *Marine Hydrodynamics*. MIT Press.

PARK, H. & CHOI, H. 2012 Kinematic control of aerodynamic forces on an inclined flapping wing with asymmetric strokes. *Bioinspir. Biomim.* **7**, 016008.

POELMA, C., DICKSON, W. & DICKINSON, M. H. 2006 Time-resolved reconstruction of the full velocity field around a dynamically-scaled flapping wing. *Exp. Fluids* **41**, 213–225.

SANE, S. P. 2003 The aerodynamics of insect flight. *J. Expl Biol.* **206**, 4191–4208.

SANE, S. P. & DICKINSON, M. H. 2002 The aerodynamic effects of wing rotation and a revised quasi-steady model of flapping flight. *J. Expl Biol.* **205**, 1087–1096.

SHYY, W., TRIZILA, P., KANG, C. K. & AONO, H. 2009 Can tip vortices enhance lift of a flapping wing? *AIAA J.* **47**, 289–293.

WALKER, S. M., THOMAS, A. L. R. & TAYLOR, G. K. 2010 Deformable wing kinematics in free-flying hoverflies. *J. R. Soc. Interface* **7**, 131–142.

WANG, Z. J. 2004 The role of drag in insect hovering. *J. Expl Biol.* **207**, 4147–4155.

WEIS-FOGH, T. 1973 Quick estimates of flight fitness in hovering animals, including novel mechanisms for lift production. *J. Expl Biol.* **59**, 169–230.

WILLMOTT, A. P. & ELLINGTON, C. P. 1997*a* The mechanics of flight in the hawkmoth Manduca sexta. Part I: kinematics of hovering and forward flight. *J. Expl Biol.* **200**, 2705–2722.

WILLMOTT, A. P. & ELLINGTON, C. P. 1997*b* The mechanics of flight in the hawkmoth Manduca sexta. Part II: aerodynamic consequences of kinematic and morphological variation. *J. Expl Biol.* **200**, 2723–2745.

WU, J.-Z., MA, H.-Y. & ZHOU, M.-D. 2006 *Vorticity and Vortex Dynamics*. Springer.